Mon. Not. R. Astron. Soc. **403,** 1131–1142 (2010) doi:10.1111/j.1365-2966.2009.16160.x

Testing a new view of gamma-ray burst afterglows

M. Nardini,[1⋆] G. Ghisellini,[2] G. Ghirlanda[2] and A. Celotti[1]

[1] *SISSA – Via Beirut 2-4, 34151 Trieste, Italy*
[2] *INAF – Osservatorio Astronomico di Brera, Via Bianchi 46, 23806 Merate, Italy*

Accepted 2009 December 3. Received 2009 December 3; in original form 2009 May 21

ABSTRACT

The optical and X-ray light curves of long gamma-ray bursts (GRBs) often show a complex evolution and in most cases do not track each other. This behaviour cannot be easily explained by the simplest standard afterglow models. A possible interpretation is to consider the observed optical and X-ray light curves as the sum of two separate components. This scenario requires the presence of a spectral break between these bands. One of the aims of this work is to test whether such a break is present within the observed *Swift* X-Ray Telescope energy range. We analyse the X-ray afterglow spectra of a sample of 33 long GRBs with known redshift, good optical photometry and published estimate of the host galaxy dust absorption $A_{\rm V}^{\rm host}$. We find that indeed in seven bright events a broken power law provides a fit to the data that is better than a single power-law model. For eight events, instead, the X-ray spectrum is better fitted by a single power law. We discuss the role of these breaks in connection to the relation between the host hydrogen column density $N_{\rm H}^{\rm host}$ and $A_{\rm V}^{\rm host}$ and check the consistency of the X-ray spectral breaks with the optical bands photometry. We analyse the optical to X-ray spectral energy distributions at different times and find again consistency with two components interpretation.

Key words: gamma-rays: bursts.

1 INTRODUCTION

The fast re-pointing capabilities of the *Swift* satellite (Gehrels et al. 2004) allowed us to reveal the early time afterglow behaviour of gamma-ray bursts (GRBs) and its unforeseen complexity. Several interpretation have been proposed to account for the unexpected light-curves evolution. This is often characterized by an early time steep flux decay starting after the end of the γ-ray prompt emission, followed by a shallower and a subsequent steeper decay, the latter corresponding to the typical afterglow observed in the pre-*Swift* era (see e.g. Nousek et al. 2006; Zhang et al. 2006).

Great efforts have been made to explain the origin of the shallow decay phase which can last from some hundreds up to hundred of thousand seconds as it cannot be explained in the frame of the simplest 'standard' forward shock fireball models. In Ghisellini et al. (2009, hereafter G09), we presented a summary of the proposed interpretations (see also Zhang 2007 for a review).

In the last years, the increasing number of well-sampled light curves allowed us to examine simultaneous optical and X-rays afterglow light curves of several long GRBs (e.g. Curran et al. 2009; de Pasquale et al. 2009). In G09, we analysed the broad-band optical to X-ray rest-frame temporal behaviour of a sample of 33 GRBs observed by *Swift* X-Ray Telescope (XRT) with known redshift, published host galaxy dust absorption estimate and good quality optical follow-up. In some cases, the optical and X-ray temporal evolution are very different. We proposed that the light-curves behaviour is due to the sum of two separate components. The first one is assumed to originate from a standard forward (external) shock, as described by Panaitescu & Kumar (2000). The second component is treated in a purely phenomenological way with the aim of minimizing the number of free parameters. A possible physical origin for it can be provided within the so-called 'late prompt' scenario described by Ghisellini et al. (2007). In G09, we found that this two-component modelling is able to well reproduce all of the optical and X-ray light curves of the GRBs of the sample (once the early steep decay phase and the flaring activity that sometimes appears in the X-ray light curves are excluded).

In order to test the consistency of the two components interpretation and make a first step towards a more physical scenario, it is important to verify whether the observed X-ray spectra and the optical to X-rays spectral energy distributions (SEDs) are in agreement with those predicted by the light-curves modelling.

In a scenario where the optical and the X-ray emission are due to different processes, the component accounting for the optical spectrum has to break in order not to dominate also in the X-ray band. Conversely, a break to a harder spectral index is also required towards the soft end of the X-ray component, not to interfere with the optical emission. However, a spectral break (e.g. the cooling break frequency of the synchrotron emission mechanism) between the optical and X-ray bands is sometimes expected also in the standard afterglow scenario (see e.g. figs 10 and 11 in

⋆E-mail: nardini@sissa.it

Nardini et al. 2006). In both scenarios, the spectral break can be at frequencies within the observed XRT 0.3–10 keV energy range. If this is the case, spectral fits provide not only the break frequency but also the spectral slope below it. This additional information makes these events the best candidates to test the two-component light-curve modelling from a spectral point of view. If the optical and X-ray light curves are dominated by the same component, the observed optical fluxes must be consistent with the extrapolation of the X-ray low-energy spectrum. If the light curves are instead dominated by different components, the X-ray spectrum extrapolation should not significantly contribute to the observed optical flux (see Section 4 for a more detailed discussion).

In this work, we analyse the XRT spectra of the GRBs in the G09 sample to check for the presence of such a break. In order to test whether the X-ray spectral break is consistent with that seen (simultaneously) in the optical, in Section 4 we examine the optical to X-ray SEDs sampled at different times along the light curves. Such a combined analysis of broad-band light curves and optical to X-ray SEDs represents a crucial consistency check for our proposed interpretation.

As discussed in Section 3.3, an interesting outcome of the spectral analysis is related to the apparent 'discrepancy' between the amount of the X-ray absorption (as measured by the hydrogen column density $N_{\rm H}^{\rm host}$) and the optical extinction $A_{\rm V}^{\rm host}$ in the host frame. The value of $N_{\rm H}^{\rm host}$ inferred from fitting the X-ray spectra with a single power law is often at odds (for standard gas-to-dust conversions) with the relatively small $A_{\rm V}^{\rm host}$ evaluated through the analysis of the optical SEDs (see e.g. Galama & Wijers 2001; Stratta et al. 2004; Kann, Klose & Zeh 2006; Schady et al. 2007a). If the intrinsic X-ray spectrum can be well modelled by a broken power law, then the required $N_{\rm H}^{\rm host}$ is smaller than that required by a single power-law fit, ameliorating the $N_{\rm H}^{\rm host}$–$A_{\rm V}^{\rm host}$ disagreement.

2 THE SAMPLE

The sample comprises the 33 long GRBs considered in G09, whose selection criteria were the knowledge of the GRB redshift, a good photometric coverage, *Swift* XRT observations and a published estimate of the host galaxy dust absorption $A_{\rm V}^{\rm host}$. When different values of $A_{\rm V}^{\rm host}$ are reported in the literature, we chose the estimate derived from a direct analysis of the optical SED rather than that obtained by a combined analysis of the optical to X-ray SEDs. If only the latter is available we discuss the effects of possible alternative solutions, through a direct analysis of the SEDs (see Section 4).

3 XRT DATA REDUCTION AND SPECTRAL ANALYSIS

We analysed the XRT data of the events in the sample with the *Swift* software package v2.9 distributed with HEASOFT (v6.6). The XRT data were reprocessed with the XRTPIPELINE tool.[1] The spectra were extracted in both WT and PC mode with the standard grade, applying, when required, the correction for pileup (Moretti et al. 2005; Romano et al. 2006; Vaughan et al. 2006). The extraction was in boxes (WT mode) or circular regions (PC mode) of typical widths as discussed in Evans et al. (2009). Background spectra were extracted in same-sized regions far from the source. For all of the spectra, we created Ancillary Response Files with the XRTMKARF tool and used the calibration data base updated to 2008 December. The spectra were rebinned in order to have a minimum of 20 counts per energy bin (15 for the faintest events) and energy channels below 0.3 keV and above 10 keV were excluded from the analysis. The XSPEC(v11.3.2) software was utilized for the analysis. For bursts with particularly bright X-ray emission, we also performed a time-resolved spectral analysis in order to check for the possible spectral evolution. Since we are not considering XRT data that are simultaneous to the Burst Alert Telescope (BAT) γ-ray detection, the steep early time phase and the flaring activity are not considered.

3.1 Single absorbed power-law model

Following the conventional analysis of X-ray GRB spectra, we fitted all the spectra with a model composed by a power law with two absorption components at low energies, wabs and zwabs. The first one corresponds to Galactic absorption and its column density $N_{\rm H}^{\rm gal}$ is fixed to the Galactic value (from Kalberla et al. 2005). The second absorption is due to the material located at the redshift of the source and its column density $N_{\rm H}^{\rm host}$ is let free to vary. The 90 per cent confidence intervals on the best-fitting parameters are obtained with the ERROR command in XSPEC. All the spectra returned a good fit with such a model, with χ^2/d.o.f close to unity. The best-fitting parameters are in a good agreement both with the results of the automatic XRT data analysis tool available online[2] developed by Evans et al. (2008, 2009) and with the values reported in the literature (summarized also in table 1 of G09). The results of the fits are reported in Table 1.

3.2 Broken power-law model

In order to test for the presence of possible spectral breaks within the XRT energy range, we selected the GRBs whose spectra have high signal-to-noise ratio (S/N), namely those which, after the applied rebinning, had a minimum of 50 energy bins. This choice, on average, corresponds to a minimum of 1000 counts per spectrum. We found 20 events fulfilling this condition. In the excluded 13 cases (i.e. GRB 050319, GRB 050408, GRB 050525A, GRB 050801, GRB 050824, GRB 051111, GRB 060512, GRB 060526, GRB 060904B, GRB 060927, GRB 070125, GRB 071010A and GRB 080310), the spectrum in the considered time intervals has too low S/N for fitting a broken power-law model which has two more free parameters (i.e. the spectral index of the second power-law component and the energy break between the two power laws) with respect to the single power-law model with galactic and intrinsic absorption.

We used two absorption components for the broken power-law models, as described in Section 3.1. The break energy $E_{\rm b}$ between the low- and high-energy power-laws spectral indices ($\beta_{\rm X,1}$ and $\beta_{\rm X,2}$, respectively) was left free to vary in the 0.3–10 keV energy range. Clearly, a significant broken power-law fit should result in statistically different $\beta_{\rm X,1}$ and $\beta_{\rm X,2}$. Therefore, no pre-determined relation between the model parameters was assumed [as done for instance if the emission process is assumed to be synchrotron ($\beta_{\rm X,1} = \beta_{\rm X,2} - 0.5$)].

The broken power law with a free rest-frame $N_{\rm H}^{\rm host}$ model (hereafter ABP) has five free parameters while the absorbed single power-law model (hereafter AP) has three free parameters that are a subset

[1]Part of the XRT software, distributed with HEASOFT package: http://heasarc.gsfc.nasa.gov/heasoft/

[2]http://www.swift.ac.uk/xrt_spectra/

Table 1. Results of the single power-law fitting. For each GRB we report the redshift, the time interval in which the spectrum was extracted, the unabsorbed spectral index β_X, the hydrogen column density at the host N_H^{host}, the reduced χ^2 and number of degrees of freedom, the host galaxy visual extinction A_V^{host} taken from the literature and the references for redshift and A_V^{host}.

GRB	z	t_{start}–t_{end} (s after trigger)	β_X	N_H^{host} (10^{21} cm^{-2})	χ^2_R (d.o.f)	A_V^{host} (mag)	Ref
050318	1.44	3.3×10^3–6.3×10^4	1.1 ± 0.1	0.5 ± 0.4	0.89 (80)	0.68 ± 0.36	Ber05a, Sti05
050319	3.24	5.0×10^3–1.1×10^5	1.06 ± 0.12	$4. \pm 4.$	0.76 (46)	0.11	Fyn05a, Kan09
050401	2.8992	1.3×10^2–8.5×10^3	0.88 ± 0.04	15.6 ± 1.9	1.056 (273)	0.62 ± 0.06	Fyn05b, Wat06
050408	1.2357	2.6×10^3–7.1×10^4	1.15 ± 0.16	12.2 ± 2.8	1.36 (37)	0.73 ± 0.18	Ber05b, dUP07
050416A	0.653	3.5×10^2–1.5×10^5	1.01 ± 0.11	5.8 ± 1.1	0.88(74)	0.19 ± 0.11	Cen05, Hol07
050525A	0.606	5.9×10^3–7.4×10^4	1.1 ± 0.17	2.1 ± 1.1	0.86 (32)	0.32 ± 0.2	Fol05, Kan09
050730	3.967	1.5×10^4–1.4×10^5	0.62 ± 0.08	4.8 ± 4.8	1.24 (95)	0.01 ± 0.005	Che05, Sta05
050801	1.56	6.5×10^2–5.2×10^4	0.84 ± 0.20	0 ± 0.07	0.66 (14)	0	DeP07, Kan09
050802	1.71	4.8×10^2–9.3×10^4	0.82 ± 0.06	1.8 ± 1.0	1.055 (159)	0.55 ± 0.1	Fyn05c Sch07
050820A	2.612	4.7×10^3–5.9×10^4	0.99 ± 0.06	3.3 ± 2.2	0.98 (143)	0.065 ± 0.008	Pro05, Kan09
050824	0.83	6.6×10^3–1.0×10^5	0.87 ± 0.18	0.6 ± 0.6	0.95 (32)	0.14 ± 0.13	Fyn05e, Kan09
050922C	3.221	1.1×10^2–4.5×10^2	1.02 ± 0.07	3.6 ± 2.2	1.00 (115)	0	Jak06, Kan09
051111	1.55	5.6×10^3–5.3×10^4	1.21 ± 0.19	6.1 ± 3.0	0.80 (36)	0.39 ± 0.11	Hil05, Sch07
060124	2.296	3.4×10^4–1.2×10^5	1.02 ± 0.08	7.6 ± 2.5	0.81 (107)	0	Cen06b, Mis07
060206	4.045	5.1×10^3–3.5×10^4	1.29 ± 0.15	15.3 ± 9.5	0.99 (87)	0 ± 0.02	Fyn06, Kan09
060210	3.91	3.8×10^3–5.8×10^4	1.10 ± 0.06	17.5 ± 5.0	1.017 (185)	1.1 ± 0.2	Cuc06, Cur07
060418	1.489	2.6×10^2–6.7×10^2	0.87 ± 0.09	4.2 ± 1.7	0.86 (91)	0.25 ± 0.22	Pro06, Ell06
060512	0.4428	3.7×10^3–2.3×10^5	0.97 ± 0.18	0.2 ± 0.2	1.39 (17)	0.44 ± 0.05	Blo06, Sch07
060526	3.221	7.4×10^2–7.6×10^3	0.95 ± 0.13	$6. \pm 6.$	0.59 (31)	0.04 ± 0.04	Ber06, Thö08
060614	0.125	4.4×10^3–2.8×10^4	0.79 ± 0.09	0.3 ± 0.3	0.98 (66)	0.05 ± 0.02	Pri06, Man07
060729	0.54	1.7×10^4–1.8×10^5	1.05 ± 0.02	0.9 ± 0.2	1.01 (290)	0.	Thö06, Gru07
060904B	0.703	1.0×10^3–4.1×10^4	1.10 ± 0.12	2.7 ± 1.2	0.86 (40)	0.44 ± 0.05	Fug06, Kan09
060908	2.43	1.5×10^2–1.9×10^3	0.84 ± 0.11	$2. \pm 2.$	1.09 (60)	0.055 ± 0.033	Rol06, Kan09
060927	5.47	1.0×10^2–6.1×10^3	0.9 ± 0.2	0.5 ± 0.5	0.75 (15)	0.33 ± 0.18	Fyn06b, RuV07
061007	1.26	2.0×10^2–2.1×10^3	0.91 ± 0.02	5.6 ± 0.3	1.054 (480)	0.54 ± 0.32	Osi06, Kan09
061121	1.314	2.0×10^2–1.8×10^4	1.01 ± 0.08	7.3 ± 1.3	0.88 (121)	0.72 ± 0.06	Blo06, Pag07
061126	1.1588	1.8×10^3–1.5×10^4	0.81 ± 0.11	5.6 ± 1.2	1.08 (143)	0	Per08a, Per08a
070110	2.352	4.0×10^3–4.5×10^4	1.12 ± 0.07	2.6 ± 1.5	0.875 (129)	0.08	Jau07, Tro07
070125	1.547	4.7×10^4–1.3×10^5	0.97 ± 0.2	1.7 ± 1.7	0.88 (21)	0.11 ± 0.04	Fox07, Kan09
071003	1.604	2.2×10^4–4.2×10^4	1.95 ± 0.12	0.7 ± 0.7	1.20 (47)	0.209 ± 0.08	Per08b
071010A	0.98	3.4×10^4–9.1×10^4	1.43 ± 0.5	13.5 ± 7.0	0.52 (11)	0.615 ± 0.15	Pro07, Cov08a
080310	2.42	1.7×10^4–5.2×10^4	0.85 ± 0.1	3.0 ± 3.0	1.11 (36)	0.1 ± 0.05	Pro08, PeB08
080319B	0.937	5.6×10^2–1.7×10^3	0.80 ± 0.01	1.6 ± 0.1	1.35 (610)	0.07 ± 0.06	Vre08, Blo09

Note. References: Ber05a: Berger, Gladders & Oemler (2005a); Sti05: Still et al. (2005); Fyn05a: Fynbo et al. (2005a); Kan08: Kann et al. (2009); Fyn05b: Fynbo et al. (2005b); Wat06: Watson et al. (2006); Ber05b: Berger, Gladders & Oemler (2005b); dUP07: de Ugarte Postigo et al. (2007); Cen05: Cenko et al. (2005); Hol07: Holland et al. (2007); Fol05: Foley et al. (2005); Che05: Chen et al. (2005); Sta05: Starling, Vreeswijk & Ellison (2005); DeP07: de Pasquale et al. (2007); Fyn05c: Fynbo et al. (2005c); Sch07: Schady et al. (2007a); Pro05: Prochaska et al. (2005); Fyn05e: Fynbo et al. (2005e); Jak06: Jakobsson et al. (2006); Hil05: Hill et al. (2005); Cen06b: Cenko, Berger & Cohen (2006b); Mis07: Misra et al. (2007); Fyn06: Fynbo et al. (2006a); Cuc06: Cucchiara, Fox & Berger (2006); Cur07: Curran et al. (2007); Pro06: Prochaska et al. (2006); Ell06: Ellison et al. (2006); Blo06: Bloom et al. (2006a); Ber06: Berger & Gladders (2006); Tho08: Thöne et al. (2008) Pri06: Price, Berger & Fox (2006); Man07: Mangano et al. (2007); Thö06: Thöne et al. (2006); Gru07: Grupe et al. (2007); Fug06: Fugazza, D'Avanzo & Malesani (2006); Rol06: Rol et al. (2006); Fyn06b: Fynbo et al. (2006b); RuV07: Ruiz-Velasco et al. (2007); Osi06: Osip, Chen & Prochaska (2006); Mun07: Mundell et al. (2007); Blo06: Bloom, Perley & Chen (2006b), Pag07: Page et al. (2007); Per08a: Perley et al. (2008a); Jau07: Jaunsen et al. (2007); Tro07: Troja et al. (2007), Fox et al. (2007); Per08b: Perley et al. (2008b); Pro07: Prochaska et al. (2007); Cov08: Covino et al. (2008); Pro08: Prochaska et al. (2008); PeB08: Perley & Bloom (2008); Vre08: Vreeswijk et al. (2008); Blo09: Bloom et al. (2009).

of the ABP model ones. Models are nested with a progression of two free parameters so an ABP model fitting is considered an improvement of the AP model one if $\Delta\chi^2 = \chi^2_{AP} - \chi^2_{ABP} > 4.6$ (90 per cent confidence). A similar choice was also done by Butler & Kocevski (2007): they considered as acceptable a more complex model (with an additional free parameter) if $\Delta\chi^2 > 2.7$.

In seven events (i.e. GRB 050802, GRB 050820A, GRB 060210, GRB 060729, GRB 061007, GRB 061126 and GRB 080319B), the fit with the ABP model resulted in an acceptable χ^2/d.o.f and the five free parameters of the ABP model were constrained with acceptable uncertainties (i.e. a χ^2 minimum is found inside the parameters definition range also considering their uncertainties). Usually both the high-energy photon index ($\beta_{X,2}$) and E_b are well constrained (typical errors of about 0.1 for the spectral index $\beta_{X,2}$ and 0.15 keV for the break energy E_b while $\beta_{X,1}$) and N_H^{host} are affected by larger, but still acceptable uncertainties (about 0.2 and 50 per cent, respectively) (see Table 2). For all the seven events, the improvement of the ABP fit with respect to the AP one yields at least a 90 per cent significant improvement.

In eight cases (i.e. GRB 050318, GRB 050401, GRB 050416A, GRB 050922C, GRB 060614, GRB 060908, GRB 070110 and GRB 071003), the ABP model is not preferred to the AP one, either because $\beta_{X,1}$ is equal to $\beta_{X,2}$ within their errors or E_b results outside the considered energy range.

In five GRBs (i.e. GRB 060124, GRB 060206, GRB 061121, GRB 050730 and GRB 060418), although the χ^2 of the ABP model is lower than that of the AP model, the improvement of the fit is not statistically significant.

Table 2. Results of the fit to the X-ray spectra with the absorbed broken power law for the seven bursts for which the model parameters are constrained. Note that β represents the energy spectral index ($\beta = \Gamma - 1$). The analysed spectra have been extracted in time intervals as in the third column of Table 1.

GRB	z	$N_{\rm H}^{\rm host}$ (10^{21} cm^{-2})	$\beta_{\rm X,1}$	$E_{\rm b}$ (keV)	$\beta_{\rm X,2}$	$\chi^2_{\rm R}$ (d.o.f)	Prob
050802	0.55	0.6 ± 0.6	$0.58^{+0.13}_{-0.14}$	$1.64^{+0.63}_{-0.64}$	0.95 ± 0.12	0.99 (157)	$6.5e^{-3}$
050820A	2.612	$2.2^{+2.2}_{-2.2}$	$0.63^{+0.15}_{-0.20}$	$1.05^{+0.70}_{-0.33}$	1.00 ± 0.07	0.947 (141)	$7.7e^{-2}$
060210	3.91	$4.^{+7}_{-4}$	$0.59^{+0.32}_{-0.22}$	$1.15^{+0.23}_{-0.17}$	1.12 ± 0.07	0.99 (183)	$8.5e^{-2}$
060729	0.54	$0.^{+0.2}_{-0}$	$0.53^{+0.24}_{-0.09}$	$1.13^{+0.13}_{-0.10}$	1.04 ± 0.04	0.97 (288)	$2.9e^{-3}$
061007	1.26	$3.0^{+0.9}_{-0.9}$	$0.02^{+0.36}_{-0.34}$	$0.80^{+0.04}_{-0.05}$	0.86 ± 0.02	1.02 (478)	$3.9e^{-4}$
061126	1.1588	$1.7^{+3.6}_{-1.7}$	$-0.16^{+0.82}_{-1.2}$	$1.05^{+0.27}_{-0.21}$	0.74 ± 0.08	1.056 (141)	$9.8e^{-2}$
080319B	0.937	$0.7^{+0.2}_{-0.2}$	$0.49^{+0.08}_{-0.10}$	$1.14^{+0.08}_{-0.08}$	0.81 ± 0.01	1.27 (608)	$8.6e^{-9}$

We re-analysed the spectra of these five events assuming an ABP model with four parameters, namely with $N_{\rm H}^{\rm host}$ frozen to the value estimated from $A_V^{\rm host}$ assuming the $A_V^{\rm host}$–$N_{\rm H}^{\rm host}$ relation reported by Schady et al. (2007a) (their equations 1, 2 or 3). For each burst, we choose the conversion corresponding to the extinction curve adopted to obtain the $A_V^{\rm host}$ from the analysis of its optical SED.

In Table 3, we report the best X-ray spectral fit parameters values for these five events and the related $\chi^2_{\rm R}$. For all of these events, we obtain a good fit to the data with $\chi^2_{\rm R}$ values close to unity like in the AP case.

As the AP parameters are no more a subset of the parameters of this model (i.e. they are not nested models), the $\Delta\chi^2$ does not provide statistical information on the fit improvement (e.g. Protassov et al. 2002).

No a priori relation between $\beta_{X,1}$ and $\beta_{X,2}$ was assumed and the extremely hard $\beta_{X,1}$ obtained for GRB 061121 and GRB 060418 cannot be easily accounted for by the standard emission processes. Given the uncertainties in the inferred $N_{\rm H}^{\rm host}$, we then fixed or constrained the value of $\beta_{X,1}$ in two ways, assuming (i) the relation $\Delta\beta = \beta_{X,1} - \beta_{X,2} = 0.5$; (ii) $\beta_{X,1} = 0$. In both cases, the best fit returns the same $\chi^2_{\rm red}$ value. For GRB 061121, the derived columns are $N_{\rm H}^{\rm host} = 0.58^{+0.20}_{-0.13} \times 10^{22}$ cm^{-2} ($\Delta\beta = 0.5$) and $N_{\rm H}^{\rm host} = 0.44^{+0.32}_{-0.13} \times 10^{22}$ cm^{-2} ($\beta_{X,1} = 0$), while for GRB 060418 $N_{\rm H}^{\rm host} = 0.28^{+0.2}_{-0.16} \times 10^{22}$ cm^{-2} ($\Delta\beta = 0.5$) and $N_{\rm H}^{\rm host} = <0.25 \times 10^{22}$ cm^{-2} ($\beta_{X,1} = 0$). We conclude that for these two bursts the data cannot robustly constrain the low-energy spectral slope as an acceptable fit can be obtained for not so extreme values of $\beta_{X,1}$. The column densities obtained in these cases are intermediate between the ones obtained through the ABP and the AP models, in agreement with those found by Schady et al. (2007a) when assuming $\Delta\beta = 0.5$.

3.3 Discussion on the X-ray spectral analysis

The breaks that we have found are all in the range between 0.6 and 1.6 keV. This is likely due to the fact that the peak of the effective area of the *Swift*-XRT is 1.5 keV and it is therefore easier to find a spectral break when it falls around this energy. A break at $E_{\rm b} < 0.6$ keV is hardly detectable and therefore we cannot exclude its presence in most of the spectra. Also a break at $E_{\rm b} > 3$ keV cannot be easily detected with the available late time X-ray spectra but we expect in this case to obtain a quite hard spectrum fitting with an AP model (i.e. a single power-law spectral index with a value similar to the obtained $\beta_{\rm X,1}$). Since the values of $\beta_{\rm X}$ reported in Table 1 are usually not so hard, we do not expect we are missing a large number of $E_{\rm b} > 3$ keV breaks.

It has been already pointed out (e.g. Galama & Wijers 2001; Stratta et al. 2004; Schady et al. 2007a; Starling et al. 2007; Watson et al. 2007) that the $N_{\rm H}^{\rm host}$ derived from the fit of the X-ray spectra are usually quite large (up to a few $\times 10^{22}$ cm^{-2}). On the other hand, the values inferred for host galaxy dust reddening $A_V^{\rm host}$ are usually small. This is true also for the GRBs in our sample as shown in Fig. 1.

From the observational point of view, the large $N_{\rm H}^{\rm host}$ derived from the fitting of the X-ray spectrum corresponds to a deficit of counts below approximately 1 keV with respect to the extrapolation of a single power-law model. In principle, this deficit could instead be due to an intrinsically curved or a broken power-law spectrum. For the seven GRBs for which the ABP model gave a better fit (with respect to the AP model), we can check if the obtained values of $N_{\rm H}^{\rm host}$ are in agreement with the optical extinction assuming a $N_{\rm H,X}$ versus A_V relation (e.g. equations 1, 2 or 3 in Schady et al. 2007a) $A_V^{\rm host}$. Fig. 2 shows the values of $N_{\rm H}^{\rm host}$ obtained with the

Table 3. Results of the absorbed broken power-law model fitting obtained by freezing the value of $N_{\rm H}^{\rm host}$ to that estimated from $A_V^{\rm host}$ through equation (1), (2) or (3) in Schady et al. (2007a) (see text). The analysed spectra have been extracted in time intervals as in the third column of Table 1.

GRB	z	$N_{\rm H}^{\rm host}$ (10^{21} cm^{-2})	$\beta_{\rm X,1}$	$E_{\rm b}$ (keV)	$\beta_{\rm X,2}$	$\chi^2_{\rm R}$(d.o.f)
050730	3.967	0	$0.36^{+0.23}_{-0.27}$	$1.00^{+0.6}_{-0.25}$	$0.75^{+0.09}_{-0.09}$	1.22 (94)
060206	4.045	0	$0.03^{+0.62}_{-1.4}$	$0.63^{+0.18}_{-0.11}$	$1.23^{+0.12}_{-0.12}$	0.98 (86)
060124	2.296	0	$0.47^{+0.14}_{-0.19}$	$1.27^{+0.27}_{-0.25}$	$1.05^{+0.1}_{-0.1}$	0.81 (106)
060418	1.489	0	$-0.23^{+0.5}_{-0.6}$	$0.79^{+0.2}_{-0.09}$	$0.81^{+0.08}_{-0.07}$	0.85 (90)
061121	1.314	1.44	$-0.89^{+0.46}_{-0.65}$	$0.79^{+0.09}_{-0.08}$	$0.89^{+0.06}_{-0.06}$	0.88 (120)

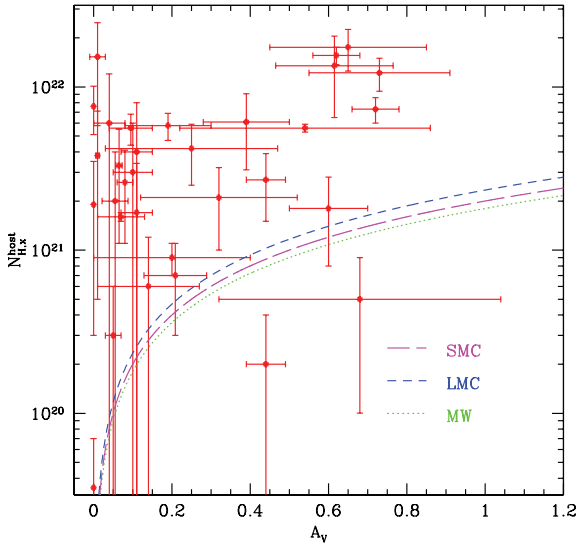

Figure 1. Rest-frame column densities $N_{\rm H}^{\rm host}$ (obtained from fitting a single power-law model to the X-ray data) versus the visual extinction $A_{\rm V}^{\rm host}$ in the GRB host galaxy for all 33 GRBs of the sample. The three curved lines correspond to the $N_{\rm H,x}$ versus $A_{\rm V}$ relations observed in the Milky Way and in the Small Magellanic Cloud as described by equations (1), (2) or (3) in Schady et al. (2007a).

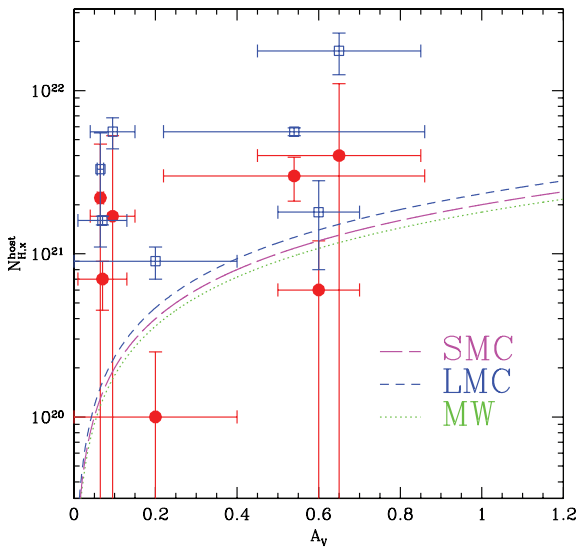

Figure 2. Rest-frame column densities $N_{\rm H}^{\rm host}$ versus visual extinction $A_{\rm V}^{\rm host}$ for the seven GRBs in which a broken power-law model gave an acceptable fit (see the text). Filled circles represent the column densities obtained from an absorbed broken power-law fit to the XRT spectra with the local absorption fixed to the Galactic $N_{\rm H}^{\rm Gal}$ values while empty squares indicate the $N_{\rm H}^{\rm host}$ obtained from a single power-law fitting for the same events. The three curved lines represent the $N_{\rm H,x}$ versus $A_{\rm V}$ relations observed in the Milky Way and in the Small Magellanic Cloud as described in Schady et al. (2007a).

ABP model fitting versus $A_V^{\rm host}$ (filled circles). For comparison, also the $N_{\rm H}^{\rm host}$ values obtained with the AP model fitting (empty squares) are reported. The solid lines represent the Milky Way and Small Magellanic Cloud like relations as in Fig. 1. For five GRBs, the uncertainties on $N_{\rm H}^{\rm host}$ are quite large, making these values consistent with zero, i.e. they must be considered as upper limits. These limits, always smaller than the $N_{\rm H}^{\rm host}$ values obtained with the AP model,

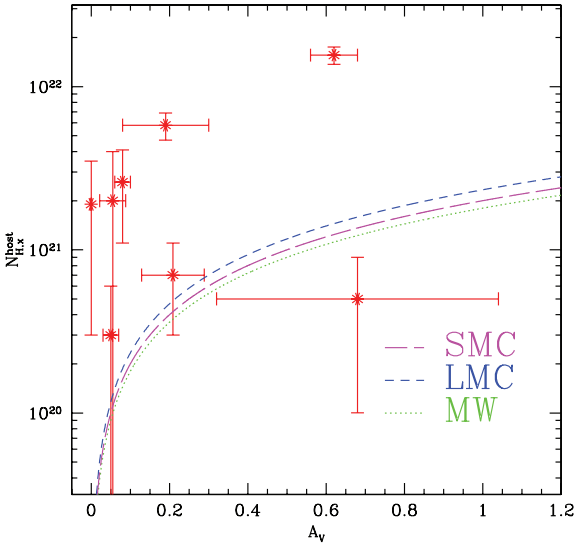

Figure 3. Rest-frame column densities $N_{\rm H}^{\rm host}$ versus the visual extinction $A_{\rm V}^{\rm host}$ obtained from the AP model for the events where the ABP model is excluded. The two curved lines represent the $N_{\rm H,x}$ versus $A_{\rm V}$ relations observed in the Milky Way and in the Small Magellanic Cloud as described in Schady et al. (2007a).

are consistent with the observed $A_V^{\rm host}$. For the remaining two GBRs (GRB 060210 and 080319B), however, the value of $N_{\rm H}^{\rm host}$ are still somewhat larger than that expected by the standard gas-to-dust relation, though clearly the disagreement is less pronounced.

While the presence of an intrinsic break in the emitted X-ray spectrum can solve or mitigate the problem of an excess of $N_{\rm H}^{\rm host}$ with respect to the optical reddening for a fraction of events, this cannot be considered as a general solution of this issue, on the basis of different indications.

As the excess is observed in a large fraction of GRBs, this would imply that the observed X-ray spectrum is almost always a broken power law, with a break in the rather narrow 0.5–1.5 keV energy range, even if the redshifts of these bursts are different.

Furthermore, we can directly exclude the presence of a spectral break inside the observed XRT spectrum for about half of the analysed events. In general, these events have an intermediate/high $N_{\rm H}^{\rm host}$ (when fitted with the AP model; see Fig. 3 compared to Fig. 2).

4 OPTICAL TO X-RAYS SEDS

In this section, we present the broad-band SEDs for the seven events in which we found a break in the X-ray spectrum to check whether the spectra, when extrapolated to lower frequencies, are consistent with the available optical photometry at the same epoch. Then the optical to X-ray SED information will be combined with the results on the decomposition of the light-curves behaviour in two components, as suggested by G09.

A key test of the two-component light-curve modelling by G09 is to verify whether the spectral properties at different times are consistent with those inferred by the light-curve de-convolution. The seven GRBs whose X-ray spectrum is consistent with the presence of a break in the X-ray band are the best candidates to perform the test as shown in Fig. 4.

For each burst, we select epochs where simultaneous optical photometry and XRT observations are available in order to use the most complete spectral information available and to avoid (if

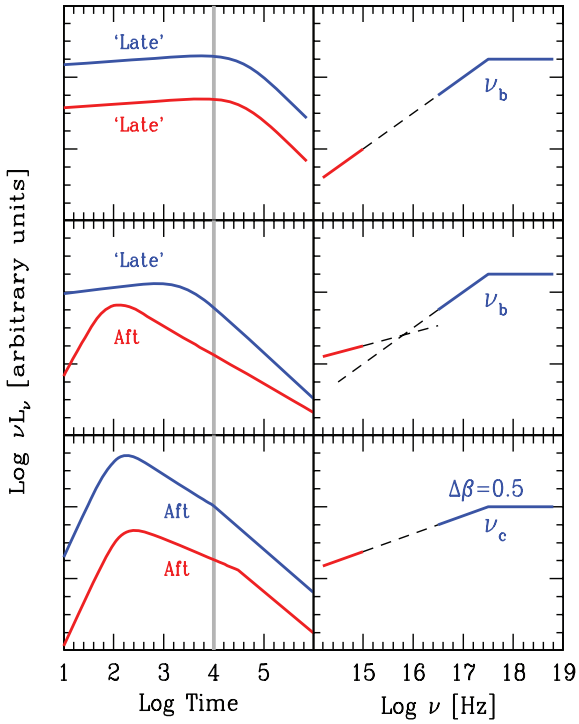

Figure 4. Sketch illustrating the possible different cases for the relation between light-curves behaviour in terms of the two-component decomposition and SEDs. The left-hand panels refer to the X-ray (upper curves) and optical (lower curves) light curves, while the corresponding expected optical to X-ray SED are shown in the right-hand panels. The bottom right-hand panel shows the standard 'afterglow–afterglow' case, i.e. both light curves are dominated by the afterglow component, with a cooling break appearing first at X-ray energies. The vertical grey line indicates the time of the extraction of the SED. ν_b and ν_c represent the break and cooling frequency, respectively.

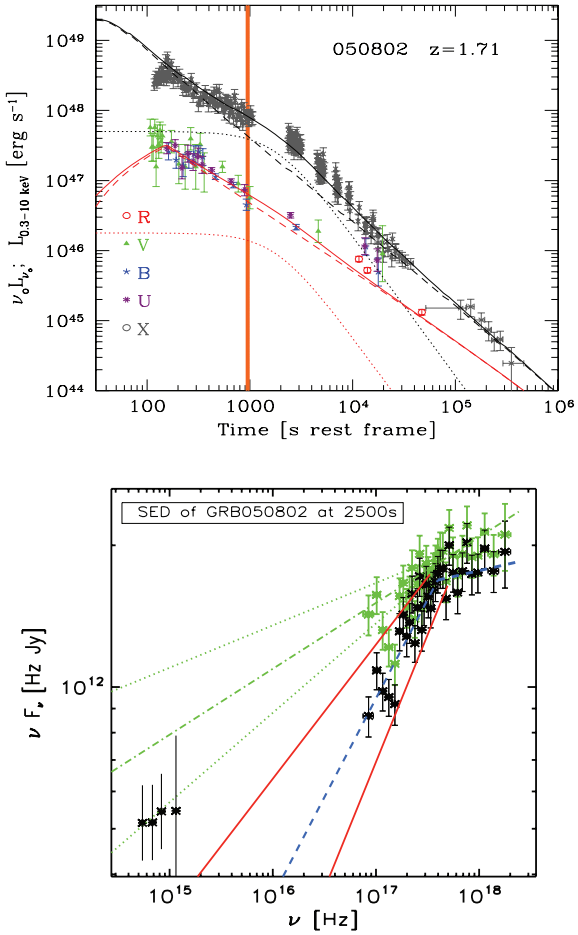

Figure 5. Top panel: X-ray (in grey) and optical (different symbols, as labelled) light curves of GRB 050802 (in the rest-frame time). Lines indicate the model fitting: afterglow component (dashed line), 'late prompt' one (dotted line) and their sum (solid line). Black lines refer to the X-rays, light grey (red in the electronic version) to the optical. The vertical line marks the time at which the SED is extracted. Bottom panel: optical to X-ray νF_ν SED at about 2500 s (observed time, corresponding to 920 s rest frame) after trigger. The dashed and solid lines show, respectively, the best fit (with the ABP model) to the X-ray spectrum (the spectral parameters are reported in Table 2) and the uncertainties on the slope of the low-energy spectral index $\beta_{X,1}$. The dotted line shows the best fit (with the AP model) to the X-ray spectrum.

possible) flux extrapolations. This limits the number of optical to X-ray SED considered.

The X-ray spectrum is extracted from a time interval around the selected epoch in order to have at least 50 energy bins and it is renormalized to the 0.3–10 keV flux obtained from the light curve. The spectral index plotted in the SEDs are the ones reported in Table 2. As done in G09, we used the light curves from the *Swift* repository (see Evans et al. 2009). The counts to flux conversion instead was done using the values from our broken power-law spectral fits. When the optical and X-ray bands light curves track each other, i.e. they are dominated by the same component, one single SED is considered; when instead they show different temporal behaviours, we considered more SEDs to test the modelling at different phases of the evolution of the two components.

In the following, we present the results for six of the seven GRBs separately. The complexity of the remaining one (i.e. GRB 080319B) prompted us to discuss it in details in a dedicated paper (Nardini et al., in preparation). We anticipate that no event shows an optical to X-rays SED that is inconsistent with the presence of a break in the XRT band and the two-component interpretation.

4.1 GRB 050802

The optical light-curve photometric data are mainly from Oates et al. (2007) together with later time *R*-band data from GRB Coordinates Networks (Pavlenko et al. 2005; Fynbo et al. 2005d). The *Swift* Ultraviolet/Optical Telescope (UVOT) filters *uvm2* and *uvw2* are strongly affected by Lyα dumping and are not considered. The X-ray light curve has been modelled as the combination of 'standard afterglow' emission dominating at early and at late times (before 700 s and after about 10 ks, rest frame) and 'late prompt' emission dominating in between. The 'standard afterglow' component instead describes the evolution of the optical flux during the whole period of the follow-up (see Fig. 5).

We extracted the optical to X-ray SED around an observed time of 2500 s (920 s rest frame) when the optical light curve is dominated by the standard afterglow and 'late prompt' emission is becoming predominant in the X-rays. The X-ray spectrum represented in Fig. 5 has been extracted in the time interval reported in Table 1. Schady et al. (2007a) estimated a non-negligible host galaxy dust absorption ($A_V^{host} = 0.55 \pm 0.1$) on the basis of a Milky Way extinction curve and assuming a power-law spectrum connecting the optical and

X-ray bands. By considering the optical bands alone, we find a similar $A_{\rm V}^{\rm host} = 0.6$ with an optical spectral index $\beta_{\rm o} \approx 0.9$.

The SED, plotted in Fig. 5, is consistent with the optical and the X-ray emission being dominated by different components [note that also Oates et al. (2007) and de Pasquale et al. (2009) found a similar inconsistency] with a spectral break falling in the observed XRT energy range, as indeed obtained from the X-ray spectral analysis. Note that the X-ray spectra shown in this section have been 'de-absorbed' both for the galactic and the host frame (when present) contributions.

4.2 GRB 050820A

The photometric data are from Cenko et al. (2006a, 2009). *Swift*/BAT triggered on a precursor about 200 s before the main event (Cenko et al. 2006a; Burlon et al. 2008). Our reference time is set at the trigger time and we do not consider the prompt X-ray emission detected before the end of the main γ-ray event. The X-ray light curve is dominated by the 'late prompt' component up to 200 ks (720 ks in the observer frame), and by a 'standard afterglow' component after then. The 'standard afterglow' emission instead prevails during the entire duration of the optical light curve but in a time interval around 5 ks (18 ks observer frame) where its contribution becomes comparable with the 'late prompt' one (see Fig. 6).

We extracted two SEDs in order to test the modelling at two different light-curve phases. The first one is at about 20 ks in the observer frame (∼5500 s rest frame) where the 'late prompt' gives the maximum contribution in the optical light curve and the available photometry is richer (I_c, R_c, V, g and B bands). Cenko et al. (2006a) estimated a $\beta_{\rm o} = 0.77$ with negligible host galaxy dust absorption while Kann et al. (2009) inferred an $A_{\rm V}^{\rm host} = 0.065 \pm 0.008$. We used the latter estimate and obtained $\beta_{\rm o} \approx 0.7$. This first SED is plotted in Fig. 6 and shows that the optical flux lies slightly above the extrapolation of the broken power law that best describes the XRT spectrum, but as the uncertainties on $\beta_{\rm X,1}$ are quite large the optical flux is fully consistent with the extrapolation. In this SED, the X-ray data are extracted from the time interval reported in Table 1.

As mentioned at 5500 s (rest frame), the optical flux is due to a similar contribution of the 'standard afterglow' and the 'late prompt' component. The cooling frequency is already redward of the considered optical bands and the 'standard afterglow' has $\beta_{\rm o} = 0.92$ (corresponding to an emitting particle distribution with slope $p = 1.85$). In the 'late prompt' component modelling, the low-energy spectral index is instead $\beta_{\rm o} = 0.45$ (see equation 3 in G09), consistent within errors with $\beta_{\rm X,1}$. The intermediate value of the observed optical slope is thus consistent with the predictions of the two-component modelling.

We considered a second SED at about 150 ks after the trigger (observer frame, corresponding to 41 ks rest frame). The plotted X-ray data are from the time-integrated spectrum of the complete second XRT observation. In this phase, the X-ray light curve is dominated by the 'late prompt' while the 'standard afterglow' dominates the optical emission. The combined SED is plotted in the bottom panel of Fig. 6 and confirms the proposed scenario: the optical data are at this time much brighter than those predicted by the extrapolation (with slope $\beta_{\rm X,1}$) of the X-ray spectrum to the optical bands . Even though at these late times there are only three available photometric points (I_c, R_c and V band) and the V-band flux is affected by a large error, the optical SED is well fitted by a softer $\beta_{\rm o} = 0.95$ that is closer to the value predicted for the 'standard afterglow' component.

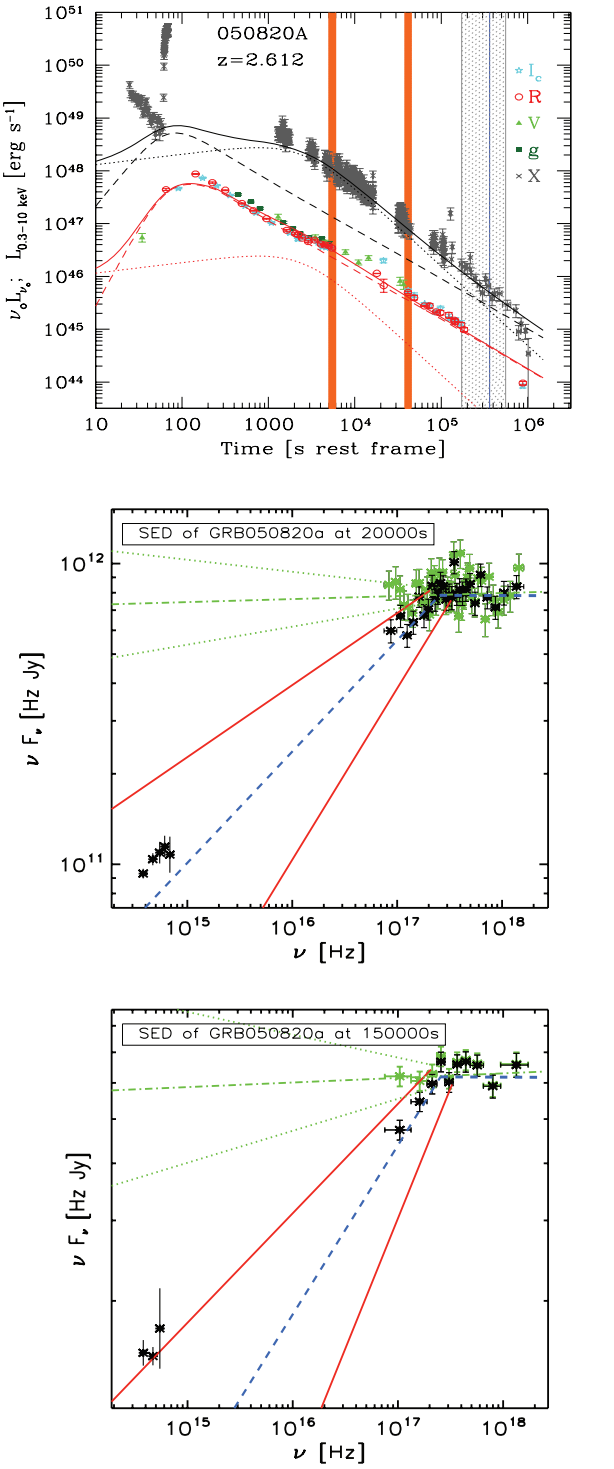

Figure 6. Top panel: X-ray and optical light curves of GRB 050820A (rest-frame time). Same notation as in Fig. 5. The thin vertical line represents the jet break time with its estimated errors (see Ghirlanda et al. 2007 and references therein). The thick vertical lines mark the times at which the SEDs are extracted. Middle and bottom panels: optical to X-ray νF_ν SED around 20 ks (middle) and 150 ks (bottom) after trigger in the observer frame (corresponding to 5.5 and 41.5 ks in the rest frame). The dashed and solid lines show, respectively, the best fit (with the ABP model) to the X-ray spectrum (the spectral parameters are reported in Table 2) and the uncertainties on the slope of the low-energy spectral index $\beta_{\rm X,1}$. The dotted line shows the best fit (with the AP model) to the X-ray spectrum.

4.3 GRB 060210

The optical afterglow has been observed in the *R* and *I* bands (photometric data from Curran et al. 2007), while, because of the high redshift, smaller wavelengths bands are not observable due to the Lyα limit. The X-ray light curve shows an intense flaring activity at early times and it is dominated by the 'late prompt' component at later times. The optical light curve is sampled only up to ∼2000 s rest frame (∼9800 s observer frame) and is dominated by the 'standard afterglow' emission, as shown in Fig. 7. Since fluxes in only two optical bands are available, it is not possible to infer the value of $A_{\rm V}^{\rm host}$ from the optical photometry. Curran et al. (2007) found a very soft observed spectrum, after correction for Galactic extinction and Lyα absorption: the optical spectral index $\beta_{\rm o}^{\rm obs} = 3.1 \pm 0.4$ at 5000 s (observer frame). Assuming that the optical and X-ray emission are produced by the same mechanism, they inferred two possible values of the host galaxy dust extinction, assuming either a single or a broken power law joining the optical and the X-ray data.

We extracted two SEDs at 4500 and 6500 s (observer frame; see Fig. 7). In both SEDs, the X-ray data are extracted from the time interval reported in Table 1. In the two-component modelling, the optical and X-ray emission would be due to different components, to account for their different temporal behaviours. Thus, $A_{\rm V}^{\rm host}$ cannot be inferred from the optical to X-rays SED. This argument, together with the fact that only two optical bands have been sampled, does not allow a direct dust absorption estimate; therefore, we do not have constraints also on the optical spectral index. If the optical emission is produced by a standard afterglow mechanism, we can choose as an example a value of $\beta_{\rm o} \approx 0.5$. If we assumed a $\beta_{\rm o} \approx 0.5$, then $A_{\rm V}^{\rm host} \approx 0.65$. Since only two optical bands are available, the uncertainties are very large but since this value is similar to the mean Small Magellanic Cloud like $E(B-V) = 0.27$ obtained by Curran et al. (2007) in the broken power-law case the latter value is used in the correction applied to the plotted SEDs. The large error on $\beta_{\rm X,1}$, and the paucity of photometric data do not allow to draw any firm conclusion on this burst.

The large uncertainties on the optical to X-ray SED at 4500 and 6500 s (observer frame), and the choice of the same $E(B-V) = 0.27$ used by Curran et al. (2007) make them consistent with a unique broken power law but the presence of two components cannot be excluded.

No break is observed in the X-ray light curve. In particular, one can estimate the expected jet break time if the GRB was to follow the so-called 'Ghirlanda relation' (Ghirlanda et al. 2007). However, the lack of evidence for such a break is consistent with the light-curve modelling as the X-ray flux is indeed dominated by the 'late prompt' emission at the time when the jet break is expected. No data are available at such a time in the optical band where such a break should have been detectable, due to the dominance of the 'standard afterglow' component.

In conclusion, the poor optical photometry of GRB 060210 does not allow to obtain an estimate of both $A_{\rm V}^{\rm host}$ and $\beta_{\rm o}$. This fact, together with the quite large errors in the $\beta_{\rm X,1}$ estimate, does not allow to infer firm conclusions on this GRB. The diversity of the optical and X-ray temporal behaviour and the lack of jet break in the late time X-ray observations prompt us to model the light curves as due to different components. The optical to X-ray SEDs cannot give better constraints to the model since within errors are consistent with both having one or two separate components.

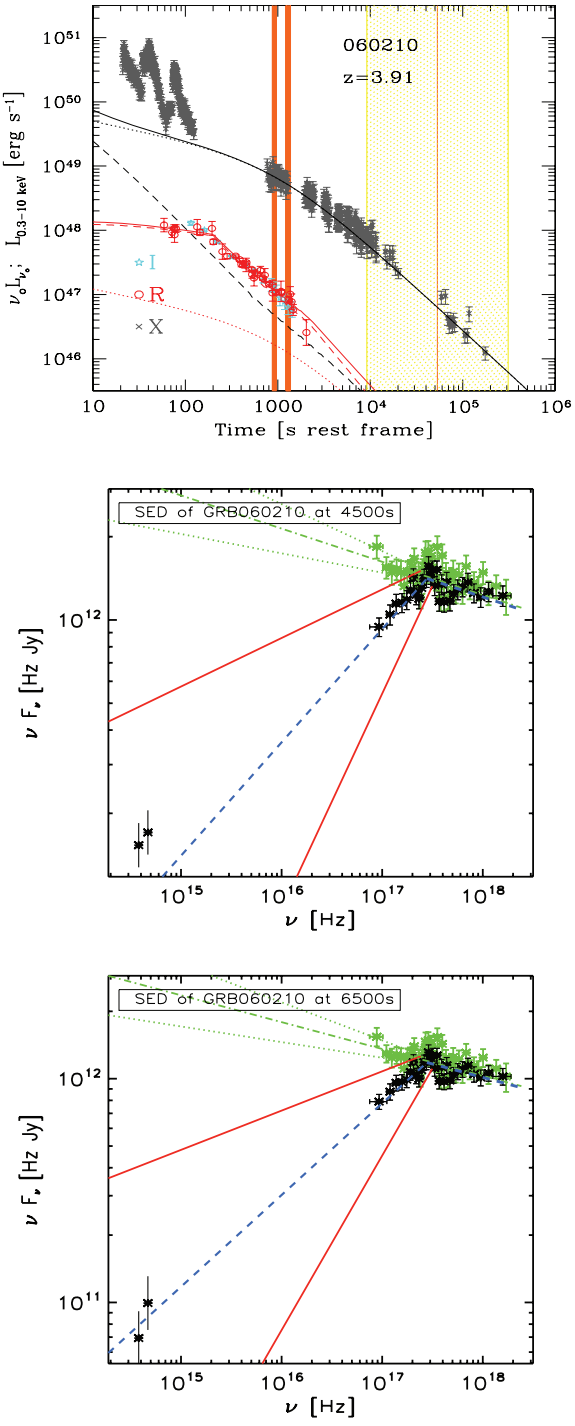

Figure 7. Top panel: X-ray (in grey) and optical (different symbols, as labelled) light curves of GRB 060210 (in the rest-frame time). Same notation as in Fig. 5. The vertical line and stripes indicate the jet times expected if the burst followed the $E_{\rm peak}$ versus E_γ 'Ghirlanda relation' (Ghirlanda et al. 2007) (see text). The vertical lines mark the time at which the SEDs are extracted. Middle (bottom) panel: optical to X-ray νF_ν SED of GRB 060210 at about 4500 (6500) s after trigger in the observer frame [916 (1300) s rest frame]. The dashed and solid lines show, respectively, the best fit (with the ABP model) to the X-ray spectrum (the spectral parameters are reported in Table 2) and the uncertainties on the slope of the low-energy spectral index $\beta_{\rm X,1}$. The dotted line shows the best fit (with the AP model) to the X-ray spectrum.

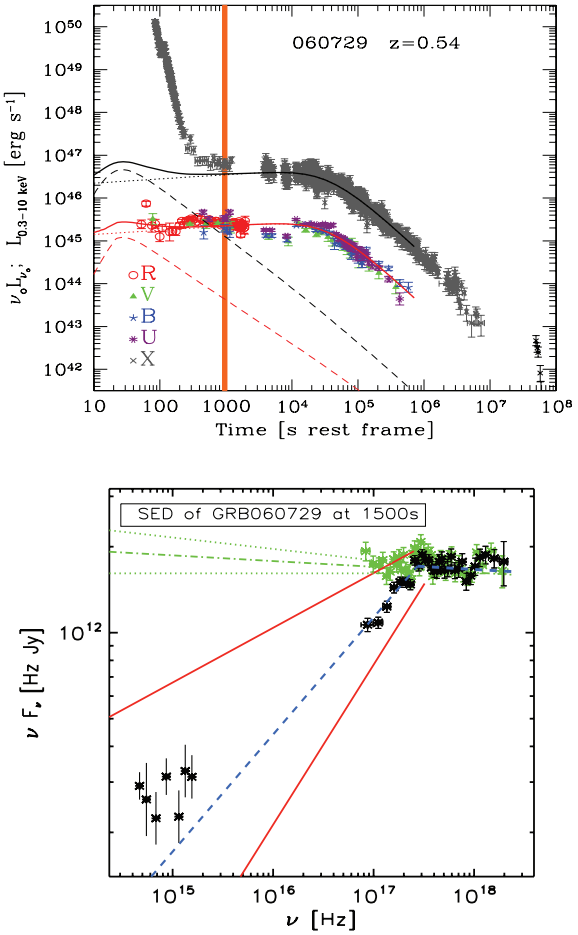

Figure 8. Top panel: X-ray (in grey) and optical (different symbols, as labelled) light curves of GRB 060729 in rest-frame time. Same notation as in Fig. 5. The vertical line represents the time at which the SED is extracted. Bottom panel: optical to X-ray νF_ν SED at about 1500 s after trigger in the observer frame (970 s rest frame). The dashed and solid lines show, respectively, the best fit (with the ABP model) to the X-ray spectrum (the spectral parameters are reported in Table 2) and the uncertainties on the slope of the low-energy spectral index $\beta_{X,1}$. The dotted line shows the best fit (with the AP model) to the X-ray spectrum.

4.4 GRB 060729

The UVOT data in six filters are from Grupe et al. (2007) while the Robotic Optical Transient Search Experiment (ROSTE) *R*-band photometry is from Rykoff et al. (2009).

After a steep decay in X-rays for about 400 s, the optical and X-rays light curves track each other and are characterized by a long-lasting (∼50 ks) shallow decay phase. Following an achromatic break, a steeper flux decay phase is observed in X-rays up to about 10^7 s after the burst (Grupe et al. 2010). The light curves are dominated by the 'late prompt' component with no significant evolution of the optical to X-ray flux ratio as can be seen in Fig. 8. As a consequence, the optical to X-ray SED is not expected to evolve in time.

The bottom panel of Fig. 8 shows that the optical flux at about 1500 s is indeed consistent with the extrapolation to the optical band of the broken power-law X-ray spectrum. The SED does not require any additional host galaxy dust absorption and the poorly constrained optical spectral index is consistent within errors with $\beta_{X,1}$. The quality of the optical–ultraviolet (UV) SED is not good enough to directly constrain the A_V^{host}.

It would be possible to consider SEDs at later times based on the UVOT data (the *R*-band photometry covers only the first XRT orbit). However, since neither the optical to X-ray flux ratio nor the colour significantly evolve, we present here only the most complete SED at 1500 s. In this case, the plotted X-ray spectrum is extracted from the first two PC mode orbits excluding the first 150 s of the first orbit in order to avoid the contribution of the steep decay phase.

4.5 GRB 061007

The photometric data are from Mundell et al. (2007) (*I*, *R*, *V* and *B* bands) and Rykoff et al. (2009) (ROTSE *R* band). After a steeper flux decay lasting about 90 s (rest frame), the X-ray light curve declines following a single power law for the whole observed time. The optical flux instead shows a fast rise (by about two orders of magnitude) in the first 40 s followed by a simple power-law decay up to about 60 ks rest frame (see Fig. 9). The first *R*-band fluxes are simultaneous with the γ-ray prompt emission, and the rise between the first and second detection is faster than t^5, hardly explainable with any standard emission mechanism.

In the two-component modelling, the optical light curve (after the end of the prompt phase, i.e. ∼50 s in the rest frame) is dominated by the 'standard afterglow' emission. The single power-law X-ray decay phase after the end of the γ-ray detection would be dominated by the 'late prompt' component. Thus, the X-ray and optical fluxes would be dominated by two different components, despite the similarity of the light curves after ∼100 s (rest frame), requiring a hard 'late prompt' $\beta_{X,1}$ in order for this emission not to significantly contribute to the observed optical flux.

The optical fluxes have been corrected for a host galaxy dust extinction $A_V^{host} = 0.54 \pm 0.30$ (Kann et al. 2009). We considered two SEDs at the times where all of the four photometric bands are simultaneously available: the first one at about 270 s (observed frame), immediately after the beginning of the simple power-law X-ray decay, and the second one at about 5.5 ks (observed frame). The X-ray data in the latter SED are extracted from the first two orbits in PC mode while the ones plotted in the first SED are extracted from the time interval reported in Table 1. In both cases, the hard $\beta_{X,1}$ found with the broken power-law fitting (see Table 2) implies a negligible contribution of the X-ray component in the optical band, supporting the proposed interpretation as can be seen from the middle and bottom panels of Fig. 9.

The X-ray light curve does not show any slope variation in correspondence to the expected jet break time obtained in the assumption that the GRB follows the 'Ghirlanda relation'. Once again this is in agreement with the 'late prompt' dominated nature of the X-ray flux. The jet break should instead be visible in the optical, but unfortunately there are no observations after 150 ks (observer frame) to confirm or rule out this prediction.

The early time optical to X-ray SEDs of GRB 061007 has been analysed also by Schady et al. (2007b) and by Mundell et al. (2007). They extracted the SED around 600 and 300 s observer frame after trigger, respectively, and they found these SEDs to be well fitted by a single power law. As can be seen in Fig. 9, the optical fluxes at 270 s (observer frame) are consistent with an extrapolation of a single power-law fit of the X-ray spectrum. Their single power-law X-ray fits give results consistent with the ones presented in Table 1. In this paper, we consider also the broad-band SED of GRB 061007 at later times. The bottom panel of Fig. 9 shows that after 5 ks the optical fluxes are no more consistent with an extrapolation of the

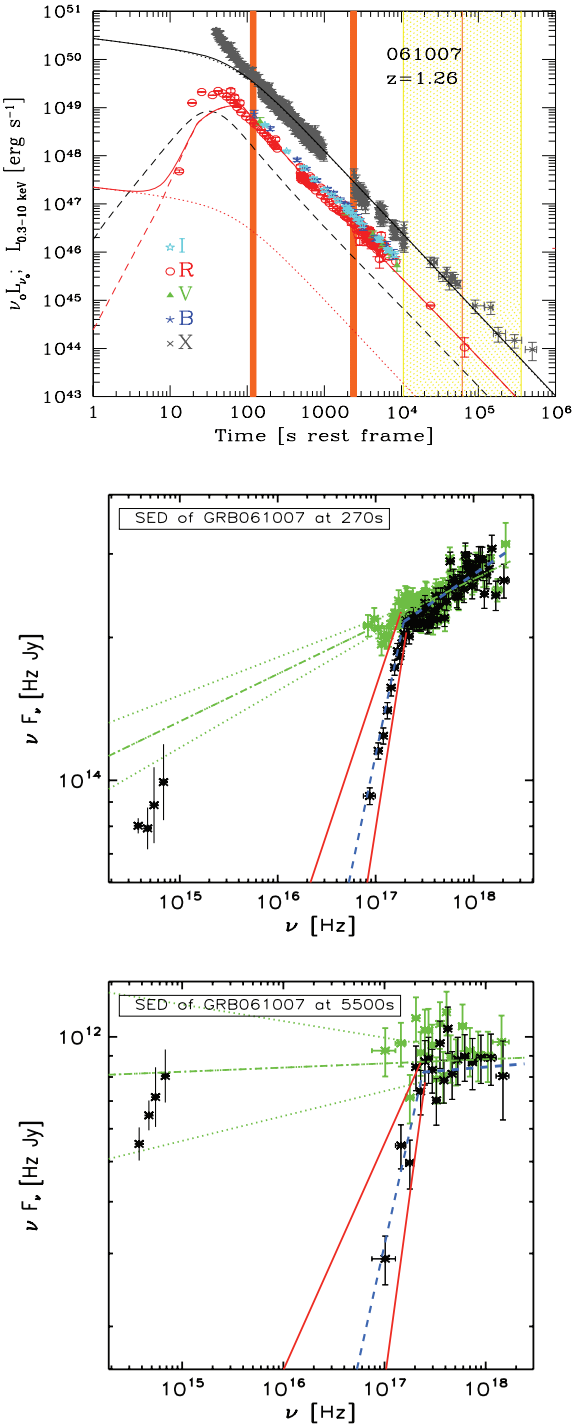

Figure 9. Top panel: X-ray and optical light curves of GRB 061007 in rest-frame time. Same notation as in Fig. 5. The vertical line and stripes indicate the jet times expected if the burst followed the $E_{\rm peak}$ versus E_γ 'Ghirlanda relation' (Ghirlanda et al. 2007) (see text). The vertical lines mark the times at which the SEDs are extracted. Middle and bottom panels: optical to X-ray νF_ν SED at about 270 (middle) and 5500 s (bottom) after trigger in the observer frame (corresponding to 120 s and 2.4 ks in the rest frame). The dashed and solid lines show, respectively, the best fit (with the ABP model) to the X-ray spectrum (the spectral parameters are reported in Table 2) and the uncertainties on the slope of the low-energy spectral index $\beta_{\rm X,1}$. The dotted line shows the best fit (with the AP model) to the X-ray spectrum.

X-ray data single power-law fit and the two-component scenario that we considered in the light-curve modelling is in good agreement with both the early and late time SEDs.

4.6 GRB 061126

A very rich photometric sampling is available for GRB 061126 (Gomboc et al. 2008; Perley et al. 2008a). After a steeper decay, the X-ray light curve follows a single power-law flux decay for the whole observed time. The infrared–optical–UV light curve instead shows a more complex behaviour, as shown in Fig. 10.

We modelled the power-law decay of the X-ray light curve as a 'late prompt' component. The optical bands is accounted for by a sudden transition from a 'standard afterglow' dominated early time to a 'late prompt' dominated late time behaviour. If correct, this scenario would imply a spectral evolution from a two components to a single component optical-to-X-ray SED. We would also expect an evolution of $\beta_{\rm o}$ at the time of transition between the two components.

We extracted two SEDs, plotted in the middle and bottom panels of Fig. 10. The first one (middle panel) corresponds to ∼2000 s (observer frame) and is obtained using eight contemporaneous photometric bands (U, B, V, R, I, J, H and $K_{\rm s}$). The X-ray data are extracted from the time interval reported in Table 1. At this time, the optical spectrum is well fitted by a single power law with $\beta_{\rm o} = 0.94 \pm 0.05$, and no host galaxy dust absorption is required. This is in agreement with the findings by Perley et al. (2008a). The optical spectrum slope is inconsistent with the X-ray spectrum. We examined a second SED at 45 ks (observer frame; bottom panel of Fig. 10) when both the optical and X-ray light curves are dominated by the 'late prompt' component. The plotted X-ray data are extracted from the time-integrated spectrum of the second XRT observation. At that time, only four optical bands are available (I_c, R_c, V and B), and the spectrum is still well fitted by a single power law without host galaxy dust absorption, but the spectral index is harder than at earlier times (i.e. $\beta_{\rm o} = 0.54 \pm 0.1$). The bottom panel of Fig. 10 reveals that not only the optical fluxes but also the optical slope are now consistent with the extrapolation from the X-rays (with slope $\beta_{X,1}$).

As predicted by the light-curve modelling, the optical spectral index evolves after the transition from standard afterglow to late prompt emission, with the SED becoming consistent with a single dominating component.

We can contrast our interpretation with the alternative one proposed by Gomboc et al. (2008), who suggested that the presence of some dust absorption at early times could account for the optical spectrum being consistent with a broken power-law optical-to-X-ray SED. At later times, the SED could be fitted with a similar broken power law but without the need of any host galaxy dust absorption. Thus, in the Gomboc et al. (2008) scenario a change in dust absorption would be required to interpret the optical spectral and broad-band SED evolution.

Also for this burst, we can evaluate the expected jet break time in the hypothesis that the GRB follows the 'Ghirlanda relation'. However, at the corresponding epoch both the optical and X-ray emission are dominated by the late prompt contribution and thus no jet break would be observable. This is indeed in agreement with the absence of a break in the observed light curves, although the observations end soon after the predicted jet break time.

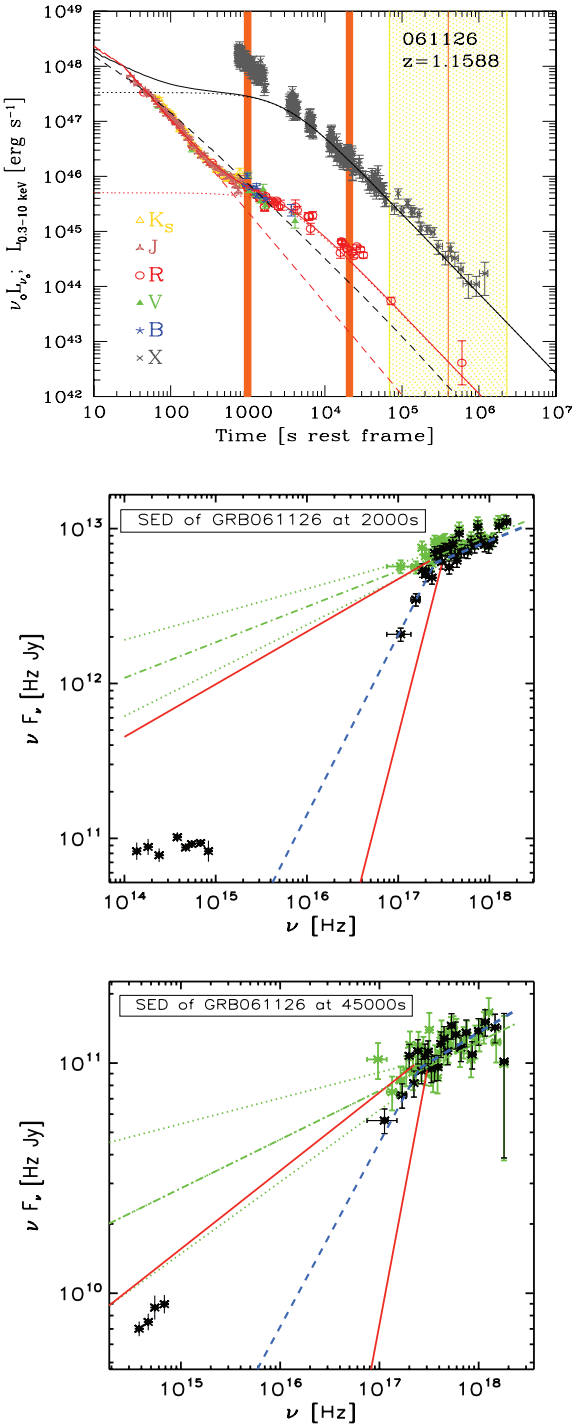

Figure 10. Top panel: X-ray (in grey) and optical (different symbols, as labelled) light curves of GRB 061126 in rest-frame time. Same notation as in Fig. 5. The vertical line and stripes indicate the jet times expected if the burst followed the $E_{\rm peak}$ versus E_γ 'Ghirlanda relation' (Ghirlanda et al. 2007) (see text). The vertical lines mark the times at which the SEDs are extracted. Middle and bottom panels: optical to X-ray ν F_ν SED at about 2200 s (middle) and 45 ks (bottom) after trigger in the observer frame (corresponding to 1000 s and 21 ks in the rest frame). The dashed and solid lines show, respectively, the best fit (with the ABP model) to the X-ray spectrum (the spectral parameters are reported in Table 2) and the uncertainties on the slope of the low-energy spectral index $\beta_{\rm X,1}$. The dotted line shows the best fit (with the AP model) to the X-ray spectrum.

5 CONCLUSIONS

We analysed the *Swift* XRT data of a sample of 33 long GRBs selected by G09 to have known redshift, published estimate of the host galaxy dust absorption and good XRT and optical follow-up.

If the XRT 0.3–10 keV spectra are modelled as a single power law, we confirm that the host frame $N_{\rm H}^{\rm host}$ column densities are rather large when compared to the values of the host galaxy dust absorption inferred from the optical analysis, according to 'standard' extinction laws (see also Stratta et al. 2004; Schady et al. 2007a).

For the 15 brightest bursts, we could model the X-ray data with a broken power law, and in seven cases we find evidence of a spectral break (90 per cent confidence level). In such cases, the required $N_{\rm H}^{\rm host}$ is in turn smaller than for the single power-law fitting and is marginally consistent with the column estimated by the optical extinction. However, in other eight bright GRBs the X-ray spectrum does not show any break and some of them do require a large value of $N_{\rm H}^{\rm host}$. Therefore, the presence of an intrinsic curvature in the spectrum cannot be considered as a general solution for the 'excess' of $N_{\rm H}^{\rm host}$ commonly found in GRB X-ray spectral analysis.

In order to test the interpretation by G09 that the X-ray and optical light-curve complex behaviour can be interpreted as due to the contributions to the emission by two different components, we combine the results of the light-curve de-convolution with the X-ray and broad-band spectral properties at different times.

In particular, we checked whether the presence of a break in the XRT spectra is consistent with what has been observed in the optical bands by studying the time-dependent optical to X-rays SEDs of the GRBs for which a spectral break was found.

We found that seven of the eight events are consistent with the presence of a break in the XRT spectra and the evolution of the broad-band SEDs appears to support the predictions of the two-components scenario, even in the presence of complex light-curve behaviours. In one case (i.e. GRB 060210), the quality of the data does not allow us to solve the ambiguity between the temporal and spectral analysis.

Consistency is also found in relation with the (lack of) evidence for jet breaks in the light curves, whose break time is estimated by assuming that the Ghirlanda relation holds for all GRBs (Ghirlanda et al. 2007). Indeed, light curves are observed to steepen in correspondence with the jet break time only when the light curve is dominated by the 'standard afterglow' emission while no break is detected if the other component is dominating.

Further testing of the two-component modelling requires to extend the simultaneous multiband optical follow-up at later times (i.e. several days after the trigger), when the typical expected *R*-band magnitudes are around 24–25. Such an intensive and long-lasting multiband follow-up could allow us (i) to search for possible optical spectral index evolution when a different component becomes dominant (as in the case of GRB 061126); (ii) to test for the presence (absence) of jet breaks in 'standard afterglow' ('late prompt') dominated optical light curves in a larger sample of events, presumably shedding light also on the jet geometry and energetics.

ACKNOWLEDGMENTS

We would like to thank Fabrizio Tavecchio for useful discussions and the anonymous referee for his interesting comments and suggestions. We acknowledge ASI grant I/088/06/0. MN and AC also acknowledge the MIUR for partial financial support. This work made use of data supplied by the UK Swift Science Data Centre at the University of Leicester.

REFERENCES

Berger E., Gladders M., 2006, GRB Coordinates Network, 5170
Berger E., Gladders M., Oemler G., 2005a, GRB Coordinates Network, 3201
Berger E., Gladders M., Oemler G., 2005b, GRB Coordinates Network, 3201
Bloom J. S., Foley R. J., Koceveki D., Perley D., 2006a, GRB Coordinates Network, 5217
Bloom J. S., Perley D., Chen H. W., 2006b, GRB Coordinates Network, 5825
Bloom J. S. et al., 2009, ApJ, 691, 723
Burlon D., Ghirlanda G., Ghisellini G., Lazzati D., Nava L., Nardini M., Celotti A., 2008, ApJ, 685, L19
Butler N. R., Kocevski D., 2007, ApJ, 663, 407
Cenko S. B., Kulkarni S. R., Gal-Yam A., Berger E., 2005, GRB Coordinates Network, 3542
Cenko S. B. et al., 2006a, ApJ, 652, 490
Cenko S. B., Berger E., Cohen J., 2006b, GRB Coordinates Network, 4592
Cenko S. B. et al., 2009, ApJ, 693, 1484
Chen H. W., Thompson I., Prochaska J. X., Bloom J., 2005, GRB Coordinates Network, 3709
Covino S. et al., 2008, MNRAS, 388, 347
Cucchiara A., Fox D. B., Berger E., 2006, GRB Coordinates Network, 4729
Curran P. A. et al., 2007, A&A, 467, 1049
Curran P. A., Starling R. L. C., van der Horst A. J., Wijers R. A. M. J., 2009, MNRAS, 395, 580
de Pasquale M. et al., 2007, MNRAS, 377, 1638
de Pasquale M. et al., 2009, MNRAS, 392, 153
de Ugarte Postigo A. et al., 2007, A&A, 462, L57
Ellison S. L. et al., 2006, MNRAS, 372, L38
Evans P. A., Osborne J. P., Burrows D. N., Barthelmy S. D., 2008, GRB Coordinates Network, 7955
Evans P. A. et al., 2009, MNRAS, 397, 1177
Foley R. J., Chen H. W., Bloom J., Prochaska J. X., 2005, GRB Coordinates Network, 3483
Fox D. B., Berger E., Price P. A., Cenko S. B., 2007, GRB Coordinates Network, 6071
Fugazza D., D'Avanzo P., Malesani D., 2006, GRB Coordinates Network, 5513
Fynbo J. P. U., Hjorth J., Jensen B. L., Jakobsson P., Moller P., Näränen J., 2005a, GRB Coordinates Network, 3136
Fynbo J. P. U. et al., 2005b, GRB Coordinates Network, 3176
Fynbo J. P. U. et al., 2005c, GRB Coordinates Network, 3749
Fynbo J. P. U. et al., 2005d, GRB Coordinates Network, 3756
Fynbo J. P. U. et al., 2005e, GRB Coordinates Network, 3874
Fynbo J. P. U., Limousin M., Castro Cerón J. M., Jensen B. L., Näränen J., 2006a, GRB Coordinates Network, 4692
Fynbo J. P. U. et al., 2006b, GRB Coordinates Network, 5651
Galama T. J., Wijers R. A. M. J., 2001, ApJ, 549, L209
Gehrels N. et al., 2004, ApJ, 611, 1005
Ghirlanda G., Nava L., Ghisellini G., Firmani C., 2007, A&A, 466, 127
Ghisellini G., Ghirlanda G., Nava L., Firmani C., 2007, ApJ, 658, 75
Ghisellini G., Nardini M., Ghirlanda G., Celotti A., 2009, MNRAS, 393, 253 (G09)
Gomboc A. et al., 2008, ApJ, 687, 443
Grupe D. et al., 2007, ApJ, 662, 443
Grupe D. et al., 2010, ApJ, 711, 1008
Hill G., Prochaska J. X., Fox D., Schaefer B., Reed M., 2005, GRB Coordinates Network, 4255
Holland S. T. et al., 2007, AJ, 133, 122
Jakobsson P. et al., 2006, A&A, 460, L13
Jaunsen A. O., Malesani D., Fynbo J. P. U., Sollerman J., Vreeswijk P. M., 2007, GRB Coordinates Network, 6010
Kalberla P. M. W., Burton W. B., Hartmann D., Arnal E. M., Bajaja E., Morras R., Pöppel W. G. L., 2005, A&A, 440, 775
Kann D. A., Klose S., Zeh A., 2006, ApJ, 641, 993
Kann D. A. et al. 2009, ApJ, submitted (arXiv:0712.2186)
Mangano V. et al., 2007, A&A, 470, 105
Misra K., Bhattacharya D., Sahu D. K., Sagar R., Anupama G. C., Castro-Tirado A. J., Guziy S. S., Bhatt B. C., 2007, A&A, 464, 903
Moretti A. et al., 2005, Proc. SPIE, 5898, 360
Mundell C. G. et al., 2007, ApJ, 660, 489
Nardini M., Ghisellini G., Ghirlanda G., Tavecchio F., Firmani C., Lazzati D., 2006, A&A, 451, 821
Nousek J. A. et al., 2006, ApJ, 642, 389
Oates S. R. et al., 2007, MNRAS, 380, 270
Osip D., Chen H. W., Prochaska J. X., 2006, GRB Coordinates Network, 5715
Page K. L. et al., 2007, ApJ, 663, 1125
Panaitescu A., Kumar P., 2000, ApJ, 543, 66
Pavlenko E., Efimov Y., Shlyapnikov A., Baklanov A., Pozanenko A., Ibrahimov M., 2005, GRB Coordinates Network, 3744
Perley D. A., Bloom J. S., 2008, GRB Coordinates Network, 7406
Perley D. A. et al., 2008a, ApJ, 672, 449
Perley D. A. et al., 2008b, ApJ, 688, 470
Price P. A., Berger E., Fox D. B., 2006, GRB Coordinates Network, 5275
Prochaska J. X., Bloom J. S., Wright J. T., Butler R. P., Chen H. W., Vogt S. S., Marcy G. W., 2005, GRB Coordinates Network, 3833
Prochaska J. X., Chen H. W., Bloom J. S., Falco E., Dupree A. K., 2006, GRB Coordinates Network, 5002
Prochaska J. X., Perley D. A., Modjaz M., Bloom J. S., Poznanski D., Chen H.-W., 2007, GRB Coordinates Network, 6864
Prochaska J. X., Murphy M., Malec A. L., Miller K., 2008, GRB Coordinates Network, 7388
Protassov R., van Dyk D. A., Connors A., Kashyap V. L., Siemiginowska A., 2002, ApJ, 571, 545
Rol E., Jakobsson P., Tanvir N., Levan A., 2006, GRB Coordinates Network, 5555
Romano P. et al., 2006, A&A, 456, 917
Ruiz-Velasco A. E. et al., 2007, ApJ, 669, 1
Rykoff E. S. et al., 2009, ApJ, 702, 489
Schady P. et al., 2007a, MNRAS, 377, 273
Schady P. et al., 2007b, MNRAS, 380, 1041
Starling R. L. C., Vreeswijk P. M., Ellison S. L., 2005, A&A, 442, L21
Starling R. L. C., Wijers R. A. M. J., Wiersema K., Rol E., Curran P. A., Koveliotu C., Van Der Horst A. J., Heemskerk M. H. M., 2007, ApJ, 661, 787
Still M. et al., 2005, ApJ, 635, 1187
Stratta G., Fiore F., Antonelli L. A., Piro L., De Pasquale M., 2004, ApJ, 608, 846
Thöne C. C. et al., 2006, GRB Coordinates Network, 5373
Thöne C. C. et al., 2008, A&A, 489, 37
Troja E. et al., 2007, ApJ, 665, L97
Vaughan S. et al., 2006, ApJ, 638, 920
Vreeswijk P. M., Smette A., Malesani D., Fynbo J. P. U., Jensen B. M., Jakobsson P., Jaunsen A. O., Ledoux C., 2008, GRB Coordinates Network, 7444
Watson D. et al., 2006, ApJ, 652, 1011
Watson D., Hjorth J., Fynbo J. P. U., Jakobsson P., Sollerman J., Wijers R. A. M. J., 2007, ApJ, 660, 101
Zhang B., 2007, Advances Space Res., 40, 1186
Zhang B. et al., 2006, ApJ, 642, 354

This paper has been typeset from a TEX/LATEX file prepared by the author.